

Low-lying electronic states of HNCS and its ions: a CASSCF/CASPT2 study

Tao Liu · Zeng-Xia Zhao · Ming-Xing Song ·
Hong-Xing Zhang · Chia-Chung Sun

Received: 8 July 2010/Accepted: 3 October 2010/Published online: 15 October 2010
© Springer-Verlag 2010

Abstract Complete active space self-consistent-field (CASSCF) and multiconfigurational second-order perturbation theory (CASPT2) calculations in conjunction with the ANO-L basis set were performed to investigate systematically the low-lying electronic states of HNCS and its ions in C_s symmetry. Our highly accurate calculation indicated that theoretically determined geometric parameters and harmonic vibrational frequencies for the ground-state X^1A' are in good agreement with observed experimental data. The geometry of triplet HNCS is clearly favored C_1 symmetry, and the relative energy is predicted to be 3.000 eV (69.2 kcal/mol). The vertical transition energies for the selected excited states of HNCS were calculated at CASSCF/CASPT2/ANO-L level of theory based on CASSCF optimized geometry. Except for a few linear states of $X^2\Pi(1^2A', 1^2A'')$, $1^4\Sigma^-(1^4A'')$, and $1^2\Sigma^+(3^2A')$ states of HNCS^+ , our results confirmed that the majority of excited states are twisted trans-bend structures. The existence of bound excited anion states has been found for the first time in HNCS^- . A more elaborate examination of ionization potential of HNCS (AIP, VIP) than previous reports has been presented.

Keywords HNCS · Excited state · CASSCF · CASPT2

Electronic supplementary material The online version of this article (doi:10.1007/s00214-010-0833-4) contains supplementary material, which is available to authorized users.

T. Liu · Z.-X. Zhao · M.-X. Song · H.-X. Zhang (✉) ·
C.-C. Sun
State Key Laboratory of Theoretical and Computational
Chemistry, Institute of Theoretical Chemistry, Jilin University,
130023 Changchun, People's Republic of China
e-mail: zhanghx@jlu.edu.cn

1 Introduction

Isothiocyanic acid (HNCS) (Fig. 1) is a well-known interstellar molecule [1–3] that always draws the attention of experimentalists [4–24] and theoreticians [22, 25–37] because of its various structure, stability, and chemical reactivity. As four-atomic closed-shell molecules, HNCS and its isomers show the similar chemical activity to halides. These chemical characteristics are widely used in fields such as organic substituents and inorganic pseudo-halide ligands [38]. In addition, HNCS and its isomers are of great use acting as important intermediates of cycloaddition reactions [23, 39]. Due to their abundant existence in the universe [1], the accurate characterization data of HNCS and its isomers, such as microwave (MV) and infrared (IR) spectra, would afford an important way to explore the unknown universe.

Among the CHNS isomers, HNCS is the most stable molecule and is now relatively well known. The gaseous HNCS was first synthesized in 1947 by heating up the mixture of KSCN and H_3PO_4 . Moreover, the structure of HNCS was first measured through the analysis of microwave rotational spectrum by Beard et al. [4]. It is notable that the NCS group was considered to be a linear fragment in this experiment. Three years later, a more accurate structure [5] was proposed by the same group. Similar figures were also derived from IR spectra [6, 7]. Later, the ultraviolet (UV) absorption spectra and the ro-vibrational of HNCS and its deuterated isotopomers were described [11, 13]. The first theoretic calculation of HNCS and its isomers was reported by Bak et al. [25]. The optimized structures and relevant energies were presented yet. In particular, the NCS group was not considered as a linear fragment any more [25], which was confirmed by series of later experimental observations [15, 40]. From then on,

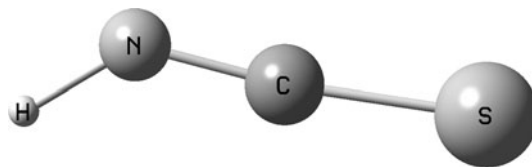


Fig. 1 The molecular geometries of ground-state HNCS

many calculations at higher levels of ab initio theories [26, 27, 29–32, 34–36] were involving in. The adiabatic ionization potential (AIP) of HNCS from photoionization was also reported (≤ 9.92 eV) [16].

Previous researches such as ab initio calculations for the [H, N, C, S] isomers substantiated the possible correlation among the four [H, N, C, S] isomers. Recently, Wierzejewska et al. [22] photolyzed HNCS in low-temperature matrices and successfully observed the existence of HSNC and HSCN. Next, the study of isomerization of HNCS on the single and triplet potential energy surface (PES) [31] was reported.

However, the electronic spectroscopy investigations of HNCS are still shorted especially in triplet or higher states. Only adiabatic ionization potential (AIP) of HNCS was calculated [9, 20, 41]. There is lack of studies on excited states of HNCS and its ions. Therefore, we focus our attentions on low-lying electronic states of HNCS and its ions in this paper. The HNCS and its ions were investigated by adopting CASSCF and CASPT2 methods, which have been proved to be an appropriate way to describe the excited electronic states of molecules and molecular ions [42–45].

2 Calculational details

The CASSCF/CASPT2 calculations were carried out using MOLCAS 6.0 [46] program package. With a CASSCF [47] wave function constituting the reference function, the CASPT2 [48] calculations were performed to compute the first-order wave function and second-order energy in the full-CI space, and multiconfigurational linear response (MCLR) [49] was used to compute harmonic vibrational frequencies. The reference wave functions and molecular orbitals have been determined by single-root CASSCF (SS-CASSCF) calculations with the given symmetry and spin.

The contracted basis sets of the Atomic Natural Orbital (ANO-L) type developed by Widmark et al. [50] was employed for H, N, C, and S atoms. Specifically, the ANO-L basis set consists of 116 contracted basis functions with a contracted scheme of H (8s4p3d/3s2p1d), C and N (14s9p4d3f/5s3p2d1f), and S (17s12p5d4f/6s4p3d1f).

Low-lying electronic states of HNCS and its ions are adopted by C_s symmetry which had been proved by

previous experimental and theoretical studies [21, 25, 31, 35]. In order to acquire accurate configuration, the active space consists of all of 13 valence orbitals (10 a' orbitals and 3 a'' orbitals), leading to 14/13 CASSCF/CASPT2 calculations (14 electrons/13 orbitals). The same active space was chosen for cationic states and anionic states, but the corresponding electrons decreased and rose by one (13/13 and 15/13) respectively. During the CASPT2 calculations, the weight values in the first-order wave functions were all larger than 0.84.

The CAS state interaction (CASSI) method [51, 52] was used to compute the transition dipole moments of the various excited states in the Frank–Condon region. These, and the CASPT2 excitation energies, were used to obtain the values of the oscillator strength. Furthermore, adiabatic ionization potentials (AIPs), vertical ionization potentials (VIPs), and adiabatic electron affinity (AEA) were investigated in our research.

3 Results and discussion

3.1 HNCS

3.1.1 Equilibrium geometries of the ground state and excited states of HNCS

The equilibrium geometries, electronic configuration, corresponding coefficients, adiabatic excitation energies, and dipole moments of the ground state and low-lying excited states were listed in Table 1. All the calculations were put at C_s symmetry, and the reference configurations (coef. ≥ 0.3) were presented in Table 1. At the CASSCF/ANO-L level, the equilibrium structure of ground-state X^1A' for HNCS was predicted to be $R_{NH} = 1.009 \text{ \AA}$, $R_{NC} = 1.206 \text{ \AA}$, $R_{CS} = 1.591 \text{ \AA}$, $\angle HNC = 134.0^\circ$, and $\angle NCS = 173.6^\circ$, respectively. By combining analysis with later listed harmonic vibrational frequencies, it is clearly seen that the geometry agrees remarkably well with the experimental conclusion: $R_{NH} = 0.9928 \text{ \AA}$, $R_{NC} = 1.2068 \text{ \AA}$, $R_{CS} = 1.5565 \text{ \AA}$, $\angle HNC = 131.7^\circ$, $\angle NCS = 173.8^\circ$ [15]. As shown in Table 1, the ground-state X^1A' has a dominant electronic configuration $(1a')^2(2a')^2(3a')^2(4a')^2(5a')^2(6a')^2(1a'')^2(7a')^2(8a')^2(9a')^2(10a')^2(11a')^2(2a'')^2(12a')^2(3a'')^2(13a')^0(4a'')^0$ with the CI coefficient of 0.95. For the sake of convenience, the symbol (core) denotes $(1a')^2(2a')^2(3a')^2(4a')^2(5a')^2(6a')^2(1a'')^2$ in the following sections. The dipole moment of the state X^1A' is 2.6 D, which is slightly larger than the B3LYP/6-311+G (d, p) value of 2.046 [35].

The states $1^3A''$, $1^3A'$, $1^1A''$, $2^1A''$, and $3^1A'$ show single configurations character and their corresponding coefficients are -0.95 , 0.96 , -0.95 , 0.92 , and -0.88 , respectively. Electron excitations from $3a''$ MO to $13a'$ MO with α and β

Table 1 Theoretical predictions of the equilibrium geometries (bond lengths are in Å, and bond angles are in °), electronic configurations, their coefficients in CASSCF wavefunction, adiabatic excitation energies T_a (in eV), and dipole moments (in Debye) for the low-lying electronic states of the HNCS at the CASSCF/CASPT2/ANO-L level

State	$R_{\text{H-N}}$ (Å)	$R_{\text{N-C}}$ (Å)	$R_{\text{C-S}}$ (Å)	\angle_{HNC} (deg)	\angle_{NCS} (deg)	Configuration ^a		T_a (CASPT2) (eV)	T_a (CASPT2) (eV)	Dipole moment (Debye)
						Occupied	Coeff.			
X^1A'	1.009	1.206	1.591	134.0	173.6	$(11a')^2(2a'')^2(12a')^2(3a'')^2(13a)^0(4a'')^0$	0.95	0.000	0.000	2.6
b	1.010	1.206	1.593	132.5	173.7					
c	1.010	1.205	1.588	133.9	173.7					
d	1.010	1.204	1.593	134.2	173.6					
B3LYP ^e	1.004	1.200	1.573	132.4	174.3					
MP2 ^e	1.004	1.210	1.572	133.2	173.5					
Exp. ^f	0.9928	1.2068	1.5565	131.7	173.8					
$1^3A(C_S)$ ^g	1.028	1.261	1.772	114.4	125.5	$(12a)^2(13a)^2(14a)^2(15a)^2(16a)^2(17a)^0$	0.95	3.265	3.000 (69.2 kcal/mol)	1.2
B3LYP ^e	1.018	1.247	1.718	119.2	124.1				67.1 kcal/mol	
$1^3A''$	1.030	1.267	1.765	112.3	128.3	$(11a')^2(2a'')^2(12a')^2(3a'')^2(13a)^2(4a'')^0$	-0.95	3.271	3.025	1.2
$1^3A'$	1.020	1.241	1.809	122.2	121.7	$(11a')^2(2a'')^2(12a')^2(3a'')^2(13a)^2(4a'')^0$	0.96	3.295	3.026	1.5
$1^1A''$	1.028	1.274	1.715	112.5	128.8	$(11a')^2(2a'')^2(12a')^2(3a'')^2(13a)^2(4a'')^0$	-0.95	3.420	3.154	1.3
$2^1A'$	1.012	1.221	1.891	135.5	111.9	$(11a')^2(2a'')^2(12a')^0(3a'')^2(13a)^2(4a'')^0$	-0.81	4.112	3.820	3.0
$2^3A'$	1.030	1.357	1.618	111.7	162.8	$(11a')^2(2a'')^2(12a')^2(3a'')^2(13a)^0(4a'')^0$	0.50			
$2^3A''$	1.007	1.410	1.719	107.8	130.8	$(11a')^2(2a'')^2(12a')^2(3a'')^2(13a)^2(4a'')^0$	0.83	5.323	4.541	1.4
$2^1A''$	1.038	1.382	1.797	110.3	95.2	$(11a')^2(2a'')^2(12a')^2(3a'')^2(13a)^2(4a'')^0$	-0.45			
$3^3A'$	0.997	1.367	1.666	123.3	139.2	$(11a')^2(2a'')^2(12a')^2(3a'')^2(13a)^2(4a'')^0$	0.81	6.258	5.586	1.7
$3^3A''$	1.007	1.408	1.768	109.4	114.5	$(11a')^2(2a'')^2(12a')^2(3a'')^2(13a)^0(4a'')^0$	-0.36			
$3^1A''$	1.020	1.354	1.722	121.5	133.2	$(11a')^2(2a'')^2(12a')^2(3a'')^2(13a)^2(4a'')^0$	0.92	6.476	5.663	1.0
$3^1A'$	1.041	1.380	1.838	106.1	102.3	$(11a')^2(2a'')^2(12a')^2(3a'')^2(13a)^0(4a'')^0$	-0.83	6.653	5.837	2.3
						$(11a')^2(2a'')^2(12a')^2(3a'')^2(13a)^2(4a'')^0$	0.36			
						$(11a')^2(2a'')^2(12a')^2(3a'')^2(13a)^0(4a'')^0$	-0.43	6.979	5.781	1.1
						$(11a')^2(2a'')^2(12a')^2(3a'')^2(13a)^2(4a'')^0$	0.42			
						$(11a')^2(2a'')^0(12a')^2(3a'')^2(13a)^2(4a'')^0$	-0.38			
						$(11a')^2(2a'')^2(12a')^2(3a'')^2(13a)^2(4a'')^0$	0.45			
						$(11a')^2(2a'')^2(12a')^2(3a'')^2(13a)^2(4a'')^0$	-0.57			
						$(11a')^2(2a'')^2(12a')^2(3a'')^2(13a)^2(4a'')^0$	-0.88	6.485	6.291	1.1

^a In active orbitals “ α ” represents a singly occupied orbital containing an electron with an up spin, “ β ” represents a singly occupied orbital containing an electron with a down spin. The common configuration [core] $(7a)^2(8a')^2(9a)^2(10a)^2$

^b Calculated at CASSCF/ANO-S

^c Calculated at CASSCF/6-311+G(3df, 3dp)

^d Calculated at CASSCF/aug-cc-pVTZ basis set. For 3A state of HNCS, the Dih(HNCS) = 158.8°

^e Taken from Ref. [15]

^f Taken from Ref. [15]

^g Dih(HNCS) = 166.6°

spin produce the $1^3A''$ and $1^1A''$ states, respectively. $3a''$ MO presents $\pi(C-S)$ bonding character and $13a'$ MO is mostly of $\pi^*(N-C-S)$ anti-bonding character. Thus, R_{CN} and R_{CS} rise up to 1.267 and 1.765 Å, and bond angles $\angle HNC$ and $\angle NCS$ decrease to 112.3° and 128.3° in the state $1^3A''$, respectively. For the same reason of electron transition in the state $1^1A''$, R_{NC} and R_{CS} are elongated by 0.068 and 0.124 Å, $\angle HNC$ and $\angle NCS$ are decreased by 21.5° and 44.8°, respectively.

The single electron transition $12a' \rightarrow 13a'$ in parallel spin happens in the state $1^3A'$ which has stretched bond lengths and decreased angles: $R_{NH} = 1.020$ Å, $R_{NC} = 1.241$ Å, $R_{CS} = 1.809$ Å, $\angle HNC = 122.2$ °, $\angle NCS = 121.7$ °. $12a'$ MO is mainly of $\pi(C-S)$ bonding character, and $13a'$ MO depicts anti-bonding character. As a result, the electron transition leads to more loosen structure state. In addition, the calculated adiabatic excitation energies of the states $1^3A''$ and $1^3A'$ are 3.025 and 3.026 eV, respectively, which means that the orbital energy interval between $12a'$ and $3a''$ is very small. The CASSCF frequency calculations for the states $1^3A''$ and $1^3A'$ at the CASSCF optimized geometry produced two imaginary frequencies of 420.9i and 775.6i (HNC bending) in the a'' symmetry, respectively. Following the vibrational mode of the imaginary frequency, we also obtained the state 1^3A at C_1 symmetry ($R_{NH} = 1.028$ Å, $R_{NC} = 1.261$ Å, $R_{CS} = 1.772$ Å, $\angle HNC = 114.4$ °, $\angle NCS = 125.5$ ° and Dih(HNCS) = 166.6°), which agrees very well with the results of Wierzejewska et al. [31]. Their computed singlet-triplet energy gap of HNCS (the X^1A' and 3A state) was 67.1 kcal/mol which is also in good agreement with our predicted value, 66.7 kcal/mol (3.000 eV).

The single electron transition $2a'' \rightarrow 13a'$ in antiparallel spin results in the state $2^1A''$. From the Fig. 2, we can find that $2a''$ MO is mainly of $\pi(N-\pi^*(C-S))$ bonding character. So after the electron transition to $13a'$ ($\pi^*(N-C-S)$) MO, R_{HN} , R_{CN} , and R_{CS} are elongated by 0.029, 0.176, and 0.206 Å, and $\angle HNC$ and $\angle NCS$ are decreased by 23.7° and

78.4°, respectively. It is notable that the dipole moment in the state $2^1A''$ is 1.0 D, which has the lowest value of dipole moments in the calculated low-lying electronic states.

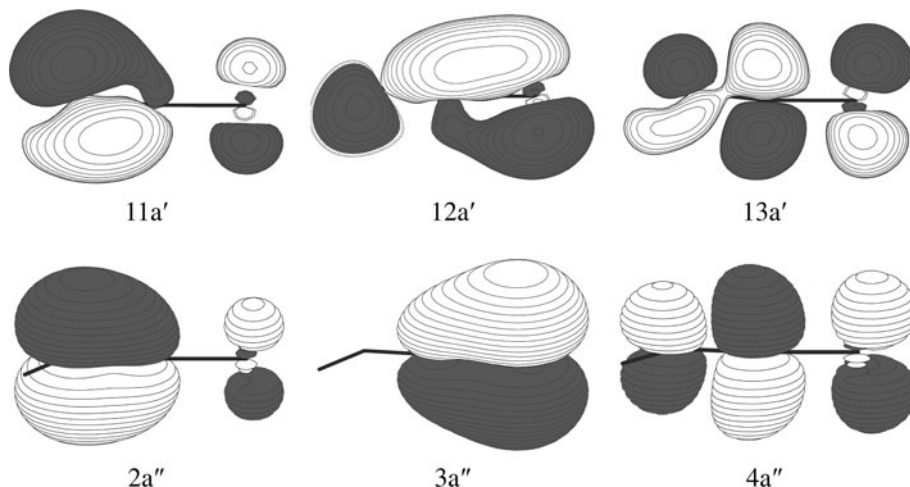
For the state $3^1A'$ one dominant doubly excited configurations, $(3a'')^2 \rightarrow (13a')^2$, contributes to the CASSCF wave function. Due to the double excitation from a bonding orbital ($\pi(C-S)$) to an antibonding ($\pi^*(N-C-S)$), R_{NH} , R_{CN} and R_{CS} are remarkably larger than that of X^1A' . Compared to the X^1A' state, $\angle HNC$ and $\angle NCS$ are decreased by 27.9 and 71.3°, respectively.

The states $2^1A'$, $2^3A'$, $2^3A''$, $3^3A'$, $3^1A''$, and $3^3A''$ show multiconfiguration character. The accompanying multi-electron transitions lead to the complicated CASSCF wave functions. The reference electrons transitions are listed in the following: $2^1A'((12a')^2 \rightarrow (13a')^2)$, $2^3A'((3a'') \rightarrow (4a'')/(12a') \rightarrow (13a'))$, $2^3A''((2a'') \rightarrow (13a')/(3a'')^2 \rightarrow (13a')(4a''))$, $3^3A'((3a'') \rightarrow (4a'')/(11a') \rightarrow (13a'))$, $3^3A''((2a'')(12a') \rightarrow (13a')^2/(2a'') \rightarrow (13a')/(3a'') \rightarrow (13a')/(2a'')^2 \rightarrow (13a')(4a''))$, $3^1A''((2a'') \rightarrow (13a')/(12a') \rightarrow (4a''))$. From the above, it is obvious that electrons excitations of HNCS almost happen in π bonding orbitals and π antibonding orbitals ($11a'$, $12a'$, $13a'$, $2a''$, $3a''$, and $4a''$). Electron transitions from bonding orbitals to anti-bonding orbitals give rise to the unstable structures with elongated bond lengths and high excited energies.

3.1.2 The harmonic vibrational frequencies of HNCS

The harmonic vibrational frequencies of 12 low-lying electronic states of HNCS were listed in Table S1 (see supporting information). There are six frequencies involved, including three types of stretching vibrational frequencies ($v_1(a')$ (H–N stretching), $v_2(a')$ (C–N stretching), and $v_3(a')$ (C–S stretch)), two types of in-plane bending vibrational frequencies ($v_4(a')$ (HNC bending) and $v_5(a')$ (NCS bending)), and one type of out-of-plane bending

Fig. 2 The plots of densities for a part of HNCS orbitals included in the active space



vibrational frequencies ($\nu_6(a'')$) (HNC bending)). The theoretical predictions of frequencies (3640.1, 2008.5, 848.4, and 592.9 cm⁻¹) are in good agreement with the experimental data [14] (3508.5, 1981.8, 850.0, and 578.0 cm⁻¹). It is clear to see that the alteration of frequencies is also consistent with the change of the geometries. The maximum value of ν_1 is 3,803.1 cm⁻¹ which is the H–N stretching vibration of the state $3^3A'$, corresponding to the shortest N–H bond length ($R_{NH} = 0.997\text{\AA}$).

3.1.3 Vertical excitation energies

Table 2 presents CASSCF/CASPT2/ANO-L calculated vertical transition energies and oscillator strengths of 11 low-lying excited states for HNCS, including five spin-allowed singlet states and six spin-forbidden triplet states.

For singlet states, the lowest excited state in energy is found to be the state $1^1A''$ with $f = 5.12 \times 10^{-4}$, which is 4.302 eV higher than the ground-state X^1A' . All the oscillator strengths for spin-allowed transitions are in the magnitude of 10^{-2} – 10^{-4} . The most intensive transition occurs at 4.803 eV ($2^1A'$), arising from $(12a')^2 \rightarrow (13a')^2$ double excitation, with $f = 2.58 \times 10^{-2}$. Furthermore, the oscillator strengths for spin-forbidden $X^1A' \rightarrow 3^3A''$ and $X^1A' \rightarrow 3^1A''$ transitions are lower than 10^{-10} . Herein, we have investigated and compared the electronic absorption spectrum proposed by Chaturvedi et al. [13]. According to their spectrum of HNCS, we averaged the wavenumbers of their identified 4 wavebands and converted them into our energy unit eV (4.012, 3.895, 4.705, 5.492 eV). We found that the comparisons to our vertical excitations: $4.012 \leftrightarrow 4.302$ ($1^1A''$, $f = 5.12 \times 10^{-4}$); $4.704 \leftrightarrow 4.803$ ($2^1A'$, $f = 2.58 \times 10^{-2}$); $5.492 \leftrightarrow 5.641$ ($2^1A''$, $f = 1.30 \times 10^{-3}$). Unfortunately, the corresponding spin-allowed

vertical excitation to the fourth value 3.895 has not been obtained yet. Through our careful investigation of their electronic spectra for HNCS, we considered that the overlap of the two indistinct bands (corresponding to 4.012 and 3.895 eV) may lead to inaccurate results. Moreover, the excitation absorption spectrum ($3^1A''$) had not been observed successfully because of their limited spectral range.

3.2 HNCS⁺ and HNCS⁻

3.2.1 Equilibrium geometries of the ground state and excited states for HNCS⁺ and HNCS⁻

The calculations of HNCS⁺ were investigated with the same basis sets and methods. Compared with the geometries of the neutral ground-state X^1A' , one electron ejection from the orbitals $12a'$ ($3\pi_x$) or $3a''$ ($3\pi_y$) leads to the degenerate states $1^2A'$ or $1^2A''$, which corresponds to the state $X^2\Pi$. As shown in Table 3, the ground-state $X^2\Pi$ ($1^2A'$, $1^2A''$) is a single-reference state with the configuration of (core) $(2\pi_x)^2(2\pi_y)^2(3\pi_x)^2(3\pi_y)^2$ (or (core) $(2\pi_x)^2(2\pi_y)^2(3\pi_x)^2(3\pi_y)^2$), and the calculated linear geometry is good consistent with the previous research [21]. The plots of densities for part of HNCS⁺ orbitals are shown in Figure S1 (see supporting information).

For the linear configuration, HNCS⁺ possesses a lowest doublet $2^2\Pi$ excited state and displays two distinctly imaginary vibrational frequencies 704.6i (in-plane) and 666.0i (out-of-plane) along the NCS bending coordinates. This is apparent that the Renner–Teller interaction has effects on the $2^2\Pi$ state. The components of the state $2^2\Pi$ with the in-plane and out-of-plane bending vibrational frequencies are assigned to trans-planar bent equilibrium structures of the states $2^2A''$ and $2^2A'$, respectively. Therefore, the state $2^2\Pi$ of HNCS⁺ is a D-type Renner–Teller molecule as proposed by Lee et al. [53]. At the CASSCF/CASPT2 level, the barriers to the states of $2^2A''$ and $2^2A'$ were predicted to be 0.159 and –0.860 eV, respectively.

The single electron excitation 3π ($\pi(C-S)$) \rightarrow 10σ ($\sigma^*(C-S)$) strongly elongates the R_{CS} (2.596 Å) for the state $1^4\Sigma^-$ ($1^4A''$) compared to the ground state of HNCS⁺. The bond interaction between C and S is apparently unstable, and the structure of $1^4\Sigma^+$ ($1^4A'$) tends to dissociate to HNC + S⁺. Owing to a single excitation from 9σ ($\pi^*(\pi(C-N)-S)$) to $3\pi_y$ ($\pi(C-S)$ bonding), the R_{CS} bond length for $1^2\Sigma^+$ ($3^2A'$) (1.624 Å) is shorter than the state $X^2\Pi$ of HNCS⁺ (1.673 Å).

For the state $2^4A''$, one dominant electron excitation configuration, $(2\pi_x) \rightarrow (4\pi_x)$ (Coef. 0.80), and one double excited configuration, $(2\pi_y)(3\pi_x) \rightarrow (2\pi_y)(4\pi_x)$ (Coef. –0.44), contribute to the CASSCF wave function. Consequently, the

Table 2 Vertical excitation energies T_v (eV) and Oscillator strengths (f) for HNCS by CASSCF/CASPT2/ANO-L

State	T_v	T_v^{exp}	f
X^1A'	0.000		
$1^3A'$	4.173	3.895 ^a	$<10^{-10}$
$1^3A''$	4.195		$<10^{-10}$
$1^1A''$	4.302	4.012 ^a	5.12×10^{-4}
$2^3A'$	4.791		$<10^{-10}$
$2^1A'$	4.803	4.705 ^a	2.58×10^{-2}
$2^3A''$	5.410		$<10^{-10}$
$2^1A''$	5.641	5.492 ^a	1.30×10^{-3}
$3^1A'$	6.510		2.63×10^{-3}
$3^3A'$	7.027		$<10^{-10}$
$3^3A''$	7.383		$<10^{-10}$
$3^1A''$	8.015		2.72×10^{-3}

^a Taken from Ref. [13]

Table 3 Theoretical predictions of the equilibrium geometries (bond lengths are in Å, and bond angles are in °), electronic configurations, their coefficients in CASSCF wavefunction, adiabatic excitation energies T_a (in eV), and dipole moments (in Debye) for the low-lying electronic states of the HNCS⁺ and HNCS⁻ at the CASSCF/CASPT2/ANO-L level

State	$R_{\text{H-N}}$ (Å)	$R_{\text{C-S}}$ (Å)	$\angle \text{HNC}$ (deg)	$\angle \text{NCS}$ (deg)	Configuration		T_a' (CASSCF) (eV)	T_a (CASSCF) (eV)	Dipole moment (Debye)
					Occupied	Coeff.			
HNCS⁺									
$X^2\Pi(1^2A', 1^2A'')$	1.016	1.160	1.673	180.0	180.0	$(2\pi_x)^2(2\pi_y)^2(3\pi_x)^2(3\pi_y)^\alpha$ (or $(2\pi_x)^2(2\pi_y)^2(3\pi_x)^\alpha(3\pi_y)^2$)	0.95	0.000 (0.000)	3.3
$1^4\Sigma^-$ ($1^4A'$)	1.010	1.165	2.596	180.0	180.0	$(2\pi_x)^2(2\pi_y)^2(3\pi_x)^\beta(3\pi_y)^\alpha$	0.96	2.269	2.369
$2^2A''$	1.027	1.235	1.854	129.0	109.2	$(11a')^2(2a')^2(12a')^0(3a')^\alpha(13a')^2(4a')^0$	-0.60	3.930	3.420
$2^2A'$	1.042	1.306	1.700	113.9	123.0	$(11a')^2(2a')^2(12a')^0(3a')^\beta(13a')^2(4a')^0$	0.54	4.438	1.2
$1^2\Sigma^+$ ($3^2A'$)	1.015	1.161	1.624	180.0	180.0	$(9\sigma)^\alpha(2\pi_x)^2(2\pi_y)^2(3\pi_x)^\beta(3\pi_y)^\alpha$	0.94	5.565	5.103
$2^4A''$	1.034	1.343	1.742	126.6	133.2	$(11a')^2(2a')^2(12a')^0(3a')^\alpha(13a')^2(4a')^0$	-0.44	6.002	5.547
$1^4A'$	1.044	1.390	1.750	109.5	129.9	$(11a')^2(2a')^2(12a')^0(3a')^\alpha(13a')^2(4a')^0$	0.80	5.803	3.4
HNCS⁻									
X^2A'	1.004	1.290	1.711	109.8	136.6	$(11a')^2(2a')^2(12a')^2(3a')^\alpha(13a')^\alpha(4a')^0$	0.96	0.000	0.000
$1^2A''$	1.009	1.307	1.647	120.8	170.4	$(11a')^2(2a')^2(12a')^2(3a')^\alpha(4a')^\alpha$	0.96	1.976	1.628
$1^4A'$	1.003	1.220	1.887	134.3	120.8	$(11a')^2(2a')^2(12a')^2(3a')^\alpha(14a')^\alpha(4a')^0$	0.96	3.278	3.663
$1^4A''$	1.011	1.250	1.806	118.1	127.6	$(11a')^2(2a')^2(12a')^2(3a')^\alpha(14a')^\alpha(4a')^0$	0.95	3.340	3.678
									13.8

R_{HN} , R_{CN} , and R_{CS} bond distances for the state $2^4\text{A}''$ are longer than those for the state $X^2\Pi$. The $\angle\text{HNC}$ and $\angle\text{NCS}$ bond angles of this state are 53.4° and 46.8° smaller than that of the ground state. Due to a single electron excitation $2\pi(\pi(\text{C-S})) \rightarrow 4\pi(\pi^*(\text{N-C-S}))$, R_{HN} , R_{CN} , and R_{CS} for the state $1^4\text{A}'$ are remarkably longer than that for the state $X^2\Pi$, and $\angle\text{HNC}$ and $\angle\text{NCS}$ are decreased.

The adiabatic electron affinity of the state $X^1\text{A}'$ yields the ground-state $X^2\text{A}'$ of HNCS^- . The state $X^2\text{A}'$ with corresponding AEA (-0.213 eV) shows that there are no stable anion states for HNCS^- . In addition, the geometry of the state $X^2\text{A}'$ is predicted to be $R_{\text{NH}} = 1.004$ Å, $R_{\text{NC}} = 1.290$ Å, $R_{\text{CS}} = 1.711$ Å, $\angle\text{HNC} = 109.8^\circ$, $\angle\text{NCS} = 136.6^\circ$. Compared to the $X^1\text{A}'$ of HNCS , the state $X^2\text{A}'$ of HNCS^- can be identified as adding an electron to the vacant $13\text{a}'$ MO of the ground state of HNCS . Therefore, the state $X^2\text{A}'$ of HNCS^- displays elongated bond lengths and decreased bond angles. In contrast to the ground state $X^1\text{A}'$ of HNCS , the state $1^2\text{A}''$ of HNCS^- with AEA of -1.841 eV has one extra electron which occupies the $4\text{a}''$ orbital ($\pi^*(\text{N-C-S})$). Thus, the electron addition elongates the R_{CN} and R_{CS} bond distances, reduces the $\angle\text{HNC}$ and $\angle\text{NCS}$. It is now generally accepted that neutral molecules with large dipole moments can form dipole-bound anion states [54–66]. Owing to its large dipole moment of 2.6 D, HNCS readily attach an ‘excess’ electron in a dipole-bound state, and so its unsaturated π -system virtually guarantees the existence of low-lying valence anion states $X^2\text{A}'$ and $1^2\text{A}''$. According to the Mulliken population analysis of the state $1^2\text{A}''$ (as shown in Table S2), the electron attachment to the $1^3\text{A}''$ and $1^3\text{A}'$ excited states give rise to the dipole-bound anion excited states $1^4\text{A}''$ and $1^4\text{A}'$ with electron affinity values of -0.865 and -0.849 eV, respectively. The extra electron in $1^4\text{A}'$ (H: 2.3723 s) and $1^4\text{A}''$ (H: 2.4509 s) states resides mainly on the positive end of the dipole of HNCS , hydrogen atom.

3.2.2 The harmonic vibrational frequencies

The frequency analysis of HNCS^+ and HNCS^- are also been performed, and related harmonical vibrational frequencies are listed in Table S3. Compared with nonlinear structures, the linear states own another out-of-plane NCS bending vibrational frequency (v_5). We note that the v_3 (a') can reflect the changes of the C–S bond lengths. For the state $1^4\Sigma^-$ of HNCS^+ , the value of v_3 (a') is 212.1 cm $^{-1}$, which is the smallest among the C–S stretching modes, which reflects the largest R_{CS} bond distance. The C–S stretching mode presents the highest C–S stretching vibrational frequency (756.5 cm $^{-1}$) for the state $1^2\Sigma^+$ ($3^2\text{A}'$), reflecting the shortest R_{CS} bond length among seven cationic states.

Table 4 Adiabatic and vertical ionization potentials (AIP and VIP) for HNCS

State	AIP		VIP	
	Calcd	Expt ^a	Calcd	Expt ^b
$1^2\text{A}''$	9.628	≤ 9.92	9.738	9.94 ± 0.02
$1^2\text{A}'$	9.628		10.073	10.3 ± 0.1
$2^2\text{A}''$	13.049		13.283	
$2^2\text{A}'$	14.067		13.316	
$1^4\text{A}''$	11.998		14.053	
$3^2\text{A}''$	13.665		14.616	
$1^4\text{A}'$	15.432		14.876	
$3^2\text{A}'$			14.916	
$2^4\text{A}'$			16.113	
$2^4\text{A}''$	15.176		16.136	
$3^4\text{A}''$			17.091	

^a Taken from Ref. [21]

^b Taken from Ref. [67]

3.2.3 The ionization potential of HNCS

The CASPT2 adiabatic and vertical ionization potentials (AIP and VIP) of HNCS are listed in Table 4. In 1994, Ruscic et al. researched on HNCS by photoionization mass spectroscopy and predicted the AIP of HNCS is ≤ 9.92 eV [14], which is consistent with our calculated value (9.628 eV). The adiabatic and vertical ionization processes from the $X^1\text{A}'$ of HNCS to the $X^2\Pi$ ($1^2\text{A}'$, $1^2\text{A}''$) of HNCS^+ need the excited energies of 9.628 (or 9.628) and 9.738 (or 10.073) eV. On the other hand, the energy gap between VIP and AIP is 0.110 (or 0.445) eV, which indicates the $12\text{a}'$ and $3\text{a}''$ MOs are bonding orbitals as mentioned earlier. The calculated first (9.7738 eV) and second (10.073) VIPs are in good agreement with the photoelectron spectrum values of 9.94 ± 0.02 eV and 10.3 ± 0.1 eV [67], respectively. The values of VIP for the states $2^2\text{A}''$, $2^2\text{A}'$, $1^4\text{A}''$, $3^2\text{A}''$, $1^4\text{A}'$ and $3^2\text{A}'$ are 13.283, 13.316, 14.053, 14.616, 14.876, and 14.916 eV, respectively. Considering the ionization energies of the five states are arranged closely, they are likely assigned to be the same energy band around 14.2 eV. Since no other bands of PES had been detected in experiments, we predict that the three bands are around 9.6, 14.2 and 16.4 eV, respectively.

4 Conclusions

Ab initio electronic structure theory (CASSCF/CASPT2) has been employed to systematically investigate low-lying electronic states of HNCS and its ions. The calculated geometric parameters and harmonic vibrational frequencies

are consistent with experimental and previously theoretical data. The electronic absorption spectra of the HNCS have been investigated by CASSCF/CASPT2/ANO-L calculations, and a series of vertical excitation energies for low-lying excited states have been obtained. The lowest vertical excitation energies are predicated at 4.302 eV for $X^1A' \rightarrow 1^1A''$ electronic transition. The first AIP at the CASSCF/CASPT2/ANO-L is 9.628 eV, which accords with the experimental value (≤ 9.92 eV). According to the VIPs values, we predicted the next bands of photoelectron spectrum around 14.2 and 16.4 eV. The adiabatic electron affinity (AEA) for HNCS is negative. Owing to large dipole moment of HNCS, all excited anion states can be characterized as dipole-bound states.

Acknowledgments This work was supported by the Natural Science Foundation of China (Grant No. 20973076).

References

- Frerking MA, Linke RA, Thaddeus P (1979) *Astrophys J* 234:143
- Irvine WM (1999) *Space Sci Rev* 90:203
- Halfen DT, Ziurys LM, Brünken S, Gottlieb CA, McCarthy MC, Thaddeus P (2009) *Astrophys J* 702:124
- Beard CI, Dailey BP (1947) *J Chem Phys* 15:762
- Beard CI, Dailey BP (1950) *J Chem Phys* 18:1437
- Jones LH, Badger RM (1950) *J Chem Phys* 18:1511
- Reid C (1950) *J Chem Phys* 18:1512
- Dousmanis GC, Sanders TM, Townes CH, Zeiger HJ (1953) *J Chem Phys* 21:1416
- Hobrock BG, Shenkel RC, Kiser RW (1963) *J Phys Chem* 67:1684
- Dillard JG, Franklin JL (1968) *J Chem Phys* 48:2353
- Krakow B, Lord RC, Neely GO (1968) *J Mol Spectrosc* 27:148
- Schettino V, Hisatsune IC (1970) *J Chem Phys* 52:9
- Chaturvedi GC, Subbaram KV, Rao DR, Rao CNR (1971) *J Mol Spectrosc* 39:242
- Draper GR, Werner RL (1974) *J Mol Spectrosc* 50:369
- Yamada K, Winnewisser M, Winnewisser G, Szalanski LB, Gerry MCL (1980) *J Mol Spectrosc* 79:295
- Polak M, Gruebele M, Saykally RJ (1987) *J Chem Phys* 87:3352
- Jacox ME (1988) *J Phys Chem Ref Data* 17:269
- Northrup FJ, Sears TJ (1990) *J Phys Chem* 93:2346
- Kambouris P, Plisnier M, Flammang R, Terlouw JK, Wentrup C (1991) *Tetrahedron Lett* 32:1497
- Brandforth SE, Kim EH, Arnold DW, Neumark DM (1992) *J Chem Phys* 98:800
- Ruscic B, Berkowitz J (1994) *J Chem Phys* 101:7975
- Wierzejewska M, Mielke Z (2001) *Chem Phys Lett* 349:227
- Wentrup C, Kambouris P (1991) *Chem Rev* 91:363
- Niedenhoff M, Yamada KMT, Winnewisser G (1997) *J Mol Spectrosc* 183:176
- Bak B, Christiansen JJ, Nielsen OJ, Svanholt H (1977) *Acta Chem Scand* 31:666
- Gimarc BM, Woodcock DA (1981) *J Mol Struc-theochem* 85:37
- Koch W, Frenking G (1987) *J Phys Chem* 91:49
- Gerbaux P, Haverbeke YV, Flammang R (1997) *J Phys Chem A* 101:6970
- Chen H-T, Ho J-J (2003) *J Phys Chem A* 107:7004
- Novak I (2003) *J Phys Chem A* 107:2743
- Wierzejewska M, Moc J (2003) *J Phys Chem A* 107:11209
- Wierzejewska M, Wieczorek R (2003) *Chem Phys* 287:169
- Wierzejewska M, Olbert-Majkut A (2003) *J Phys Chem A* 107:1928
- Pankratov AN, Khmelev SS (2005) *J Serb Chem Soc* 70:1183
- Durig JR, Zheng C, Deeb H (2006) *J Mol Struct* 784:78
- Xu J-H, Li L-C, Zheng Y, Liu J-L, Wang X (2007) *J Theor Comput Chem* 6:1
- Pasinszki T, Bazso G, Krebsz M, Tarczay G (2009) *Phys Chem Chem Phys* 11:9458
- Singh R, Dikshit SK (1995) *Polyhedron* 14:1799
- Silva S, Simão AC, Tatibouët A, Rollin P, Rauter AP (2008) *Tetrahedron Lett* 49:682
- Yamada K, Winnewisser M, Winnewisser G, Szalanski LB, Gerry MCL (1979) *J Mol Spectrosc* 78:189
- Pasinszki T, Kishimoto N, Ohno K (1999) *J Phys Chem A* 103:9195
- Martin ME, Negri F, Olivucci M (2004) *J Am Chem Soc* 126:5452
- Merchán M, Serrano-Andrés L, Robb MA, Blancafort L (2005) *J Am Chem Soc* 127:1820
- Gagliardi L, Roos BO (2007) *Chem Soc Rev* 36:893
- Liu FY, Liu YJ, Vico LD, Lindh R (2009) *J Am Chem Soc* 131:6181
- Karlström G, Lindh R, Malmqvist P-Å, Roos BO, Ryde U, Veryazov V, Widmark P-O, Cossi M, Schimmelpfennig B, Neograd P, Seijo L (2003) *Comput Mater Sci* 28:222
- Malmqvist P-Å, Rendell A, Roos BO (1990) *J Phys Chem* 94:5477
- Andersson K, Malmqvist P-Å, Roos BO, Sadlej AJ, Wolinski K (1990) *J Phys Chem* 94:5483
- McKellar ARW, Bunker PR, Sears TJ, Evenson KM, Saykally RJ, Langhoff SR (1983) *J Chem Phys* 79:5251
- Widmark P-O, Persson BJ, Roos BO (1991) *Theor Chim Acta* 79:419
- Malmqvist P-Å (1986) *Int J Quantum Chem* 30:479
- Malmqvist P-Å, Roos BO (1989) *Chem Phys Lett* 155:189
- Lee TJ, Fox DJ, Schaefer HF III (1984) *J Chem Phys* 81:356
- Lykke KR, Neumark DM, Anderson T, Trapa VJ, Lineberger WC (1987) *J Chem Phys* 87:6842
- Marks J, Brauman JI, Mead RD, Lykke KR, Lineberger WC (1988) *J Chem Phys* 88:785
- Brinkman EA, Berger S, Marks J, Brauman JI (1993) *J Chem Phys* 99:7586
- Desfrançois C, Abdoul-Carime H, Adjouri C, Khelifa N, Schermann J-P (1994) *Europhys Lett* 26:25
- Popple RA, Finch CD, Dunning FB (1995) *Chem Phys Lett* 234:172
- Abdoul-Carime H, Desfrançois C (1998) *Eur Phys J D* 2:149
- Lecomte F, Carles S, Desfrançois C (2000) *J Chem Phys* 113:10973
- Suess L, Liu Y, Parthasarathy P, Dunning FB (2003) *Chem Phys Lett* 376:376
- Hammer NI, Jordan KD, Desfrançois C, Compton RN (2003) *J Chem Phys* 119:3650
- Suess L, Liu Y, Parthasarathy P, Dunning FB (2004) *J Chem Phys* 121:7162
- Clary DC (1988) *J Phys Chem* 92:3173
- Simons J (1989) *J Chem Phys* 91:6858
- Giri PR, Gupta KS, Meijanac S, Samsarov A (2008) *Phys Lett A* 372:2967
- Cradock S, Ebsworth EAV, Murdoch JD (1972) *J Chem Soc Faraday Trans* 68:86